nature photonics

ARTICLES

https://doi.org/10.1038/s41566-019-0506-3

Generation of non-classical light in a photon-number superposition

J. C. Loredo[1,5*], C. Antón[1,5*], B. Reznychenko[2], P. Hilaire[1,3], A. Harouri[1], C. Millet[1], H. Ollivier[1], N. Somaschi[4], L. De Santis[1], A. Lemaître[1], I. Sagnes[1], L. Lanco[1,3], A. Auffèves[2], O. Krebs[1] and P. Senellart[1*]

Generating light in a pure quantum state is essential for advancing optical quantum technologies. However, controlling its photon number remains elusive. Optical fields with zero and one photon can be produced by single atoms, but, so far, this has been limited to generating incoherent mixtures or coherent superpositions with a very small one-photon term. Here, we report the on-demand generation of quantum superpositions of zero, one and two photons via coherent control of an artificial atom. Driving the system up to full atomic inversion leads to quantum superpositions of vacuum and one photon, with their relative populations controlled by the driving laser intensity. A stronger driving of the system, with 2π pulses, results in a coherent superposition of vacuum, one and two photons, with the two-photon term exceeding the one-photon component, a state allowing phase super-resolving interferometry. Our results open new paths for optical quantum technologies with access to the photon-number degree of freedom.

Controlling the photon number in a light pulse has been a primary task for enabling progress in optical quantum technologies[1,2]. Single- and *N*-photon sources[3–5] are at the heart of future quantum communication networks[6,7] and sensors[8,9], as well as optical quantum computers[10,11] and simulators[12–15]. These achievements make use of the interference of indistinguishable single photons, allowing the realization of quantum gates[16,17] and protocols such as quantum teleportation[18] and entanglement swapping[19]. The one-photon term has been exploited previously, and the vacuum component has been considered detrimental to the overall protocol efficiency, motivating a quest for deterministic sources producing single-photon Fock states with no vacuum component[20–23]—a challenging task, to say the least. If the vacuum is set, instead, in a quantum superposition with the single photon, one could use it to encode quantum information in the photon number, thus becoming a resource for optical quantum information processing. For example, vacuum within a pure quantum state can be exploited in quantum teleportation[24] or quantum random number generators[25]. However, obtaining quantum superpositions in the photon-number basis has so far demanded complex quantum-state engineering and conditioned-state preparation[26,27].

The textbook model of a quantum emitter is a two-level atom—a system shown to generate quantum light in various excitation regimes. Incoherent non-resonant excitation of natural[28] and artificial atoms[29–31] can produce optical fields with a large single-photon component, but without coherence in the photon-number basis due to the incoherent creation process of the atomic population. In contrast, coherent driving of an atom can in principle be used to transfer the coherence between the atomic ground and excited state to the emitted light field. This has so far been explored in the weak-excitation regime to produce quantum light that exhibits coherence with the driving laser, as observed with atoms[32] as well as semiconductor quantum dots[33–36]. This regime has been shown to produce squeezed light where an atomic dipole—with vanishing population—elastically scatters a coherent superposition of vacuum and a small one-photon term[37]. Generating a photon-number superposition with large single-photon population requires the creation of an atomic population, inherently coupled to its environment, that remains insensitive to any decoherence until spontaneous emission takes place. To the best of our knowledge, the generation of photon-number quantum superpositions under strong coherent driving has not been reported so far, neither with natural atoms nor with artificial ones.

In this work, we report the on-demand generation of quantum superpositions in the photon-number basis, in light pulses emitted by a single artificial atom. We observe superpositions of zero, one and two photons emitted from semiconductor quantum dots coupled to optical microcavities[20,38]. We use pulsed coherent driving, beyond full inversion of the atomic population, and perform interferometric measurements with a path-unbalanced Mach–Zehnder interferometer (MZI). As supported by our theoretical calculations, phase-dependent oscillations at the interferometer output demonstrate the production of coherent superpositions of vacuum, one and two photons. Below π-pulse driving, we obtain superpositions of vacuum and one-photon Fock states, with their relative populations controlled by the driving laser intensity. By driving the quantum dot with 2π-pulses, we obtain a state with the two-photon component larger than the one-photon population, a state allowing phase super-resolving interferometry, and incidentally resembling a small Schrödinger-cat state.

Coherent driving and photon statistics

Here, we investigate semiconductor devices consisting of a single quantum dot (QD) positioned with nanometre-scale accuracy at the centre of a connected-pillar cavity[20,39,40]. The QD layer is inserted in a p–i–n diode structure, and electrical contacts are defined to

[1]CNRS Centre for Nanoscience and Nanotechnology, Université Paris-Sud, Université Paris-Saclay, Palaiseau, France. [2]Univ. Grenoble Alpes, CNRS, Grenoble INP, Institut Néel, Grenoble, France. [3]Université Paris Diderot, Paris, France. [4]Quandela, Palaiseau, France. [5]These authors contributed equally: J. C. Loredo, C. Antón. *e-mail: juan.loredo@c2n.upsaclay.fr; carlos.anton-solanas@c2n.upsaclay.fr; pascale.senellart-mardon@c2n.upsaclay.fr

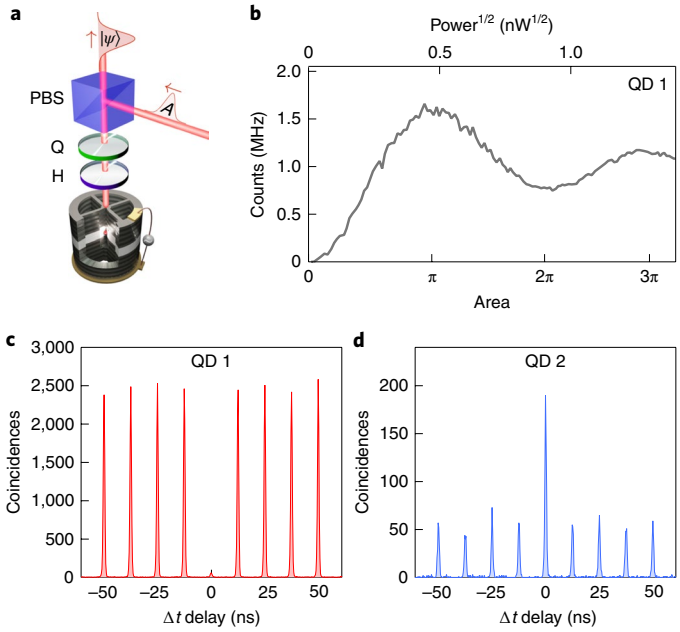

Fig. 1 | Coherent control of an artificial atom. a, Schematic of the set-up. A single semiconductor QD is kept in a cryostat at 9 K and is excited under pulsed resonant excitation. The QD emitted state $|\Psi\rangle$ is separated from the laser with pulse area A in a cross-polarization scheme by using a polarizing beamsplitter (PBS), a quarter-wave plate (Q) and a half-wave plate (H). **b**, Rabi oscillation of the QD coherent driving. The emission is collected by a single-mode fibre and directly detected with an APD. **c**,**d**, Second-order autocorrelation function $g^{(2)}(\Delta t)$ measured with π-pulse driving with QD1 (**c**) and 2π-pulse driving with QD2 (**d**).

control the QD resonance through the confined Stark effect. We note that the experimental results reported here have been observed on various QD–cavity devices. We focus hereafter on two devices: a neutral (QD1) and a charged (QD2) exciton coupled to the cavity mode (see Methods). QD1 (QD2) is excited resonantly with linearly polarized laser pulses at 925 nm, and its emission is collected using a crossed-polarization scheme that separates it from the laser (Fig. 1a). Figure 1b shows the detected count rates for QD1 as a function of the excitation pulse area A, which shows well-defined Rabi oscillations. The signal is damped by spontaneous emission due to the relatively long 40 ps excitation pulses[38] as compared to the measured emission decay time of 166 ± 16 ps. Second-order autocorrelation functions $g^{(2)}(\Delta t)$ measured along Rabi cycles evidence a distinct and complementary behaviour between π- and 2π-pulse driving. A pronounced antibunched photon statistics at the π pulse is observed for both QD1 and QD2, a signature of light wavepackets consisting mostly of either vacuum or one photon. As shown in Fig. 1c, we measure $g^{(2)}_{\pi}(0) = 0.037 \pm 0.002$ for QD1, despite using pump pulses 40 ps long compared to the emission decay time of 166 ps. Indeed, the collected signal of a neutral exciton in crossed polarization is delayed until after the excitation pulse ends due to a polarization rotation induced by exciton fine-structure splitting[38]. Such delayed collection does not take place for a charged exciton, so a shorter laser pulse duration of 15 ps, compared to the 406 ps decay time, is used to obtain $g^{(2)}_{\pi}(0) = 0.063 \pm 0.004$ with the π pulse for QD2. However, bunched statistics is observed with the 2π pulse for QD2, with $g^{(2)}_{2\pi}(0) = 2.98 \pm 0.11$ (Fig. 1d). This evidences, as recently observed[41], wavepackets containing two-photon populations. In the following, we investigate the nature of light in the photon-number degree of freedom to determine whether it contains photon Fock states emitted in a mixture or in a pure quantum state.

Quantum superposition of zero and one photon

The Hong–Ou–Mandel (HOM) effect[42] describes two single photons simultaneously impinging on a beamsplitter. If the photons are polarization, spatially and frequency indistinguishable, they bunch at the output of the beamsplitter—a behaviour exclusively of quantum mechanical origin. This requires that the interfering photons are in the same pure quantum state in these degrees of freedom.

Interference can also be used to unravel coherences in the Fock-state basis. Consider a beamsplitter with inputs a,b and outputs c,d onto which pure states of photon-number superpositions impinge. These are in the form $|\Psi_a\rangle = \sqrt{p_0}\ |0_a\rangle + \sqrt{p_1}\, e^{i\alpha}\ |1_a\rangle$ and $|\Psi_b\rangle = \sqrt{p_0}\ |0_b\rangle + \sqrt{p_1}\, e^{i(\alpha+\phi)}\ |1_b\rangle$, where $p_0 + p_1 = 1$, $p_{0,1}$ are the vacuum and one-photon populations and ϕ is the relative phase between the states. When $p_1 = 1$, their quantum interference leads to the well-known two-photon output state $(|2_c 0_d\rangle - |0_c 2_d\rangle)/\sqrt{2}$ (the HOM effect). However, as soon as $p_1 < 1$, the output state shows other photon terms that lead to a mean photon number $\mathcal{N}_{c,d} = p_1 (1 \pm p_0 \cos\phi)$ at the beamsplitter outputs (see Supplementary Information). That is, if states are pure in the photon-number basis, their interference leads to oscillations measured at the output of the interferometer device, with a visibility amplitude equal to the vacuum population p_0.

The previous example describes the idealized case of pure states—instances non-existing in the physical world. To account for impurity in the photon-number basis, we consider that each light wavepacket impinging on the beamsplitter is described by a density matrix $\rho_S = \lambda\rho_{\text{pure}} + (1-\lambda)\rho_{\text{mixed}}$, where $\rho_{\text{pure}} = |\Psi_i\rangle\langle\Psi_i|$ is a pure state ($i = a,b$), $\rho_{\text{mixed}} = \text{diag}\{p_0, p_1\}$ is a diagonal matrix and $0 \le \lambda \le 1$ is a parameter tuning the photon-number purity. Moreover, limited purity in the frequency domain is taken into account by the non-unity mean wavepacket overlap M between interfering photons. It can be shown (see Supplementary Information) that such interfering input states result in

$$n_{c,d} = \frac{1}{2}(1 \pm v\cos\phi) \tag{1}$$

where $n_{c,d} = \mathcal{N}_{c,d}/(\mathcal{N}_c + \mathcal{N}_d)$ oscillates with a visibility $v = \lambda^2 p_0 \sqrt{M}$. We observe, from equation (1), that if the interfering states are distinguishable ($M = 0$) or if the state is emitted in a statistical mixture of photon numbers ($\lambda = 0$), then v vanishes. Thus, observing $v \neq 0$ implies that neither case is true: the state contains quantum coherences in the photon-number basis.

Coherent driving of a two-level system creates a quantum superposition of ground and excited states, with a relative phase governed by the classical phase of the driving laser. If this coherence is transferred to the emitted light state through spontaneous emission, we obtain a photonic state with coherences between the vacuum and one-photon components. We test this hypothesis by performing the above described interferometric measurements. To do so, we utilize an unbalanced MZI with a path-length difference matching the temporal separation of consecutive emitted wavepackets from the quantum dot to temporally overlap them on a beamsplitter (Fig. 2a). The free-space part of the MZI leads to small path variations on the order of the photon wavelength, acting as the previously described phase ϕ (see Methods).

Figure 2b shows our measurements of $n_{c,d}$ for pulse areas $A = 0.61\pi$ and $A = 0.14\pi$. The single detector counts undergo correlated oscillations with time, as the optical phase ϕ freely evolves in time within the interferometer, evidencing quantum coherence in the photon-number basis. As predicted, the amplitude of the oscillations increases with the vacuum population, controlled here by choosing the driving pulse area. Figure 2c shows the extracted oscillation visibilities, obtained from the maxima and minima of $n_{c,d}$ with respect to ϕ, for different values of single-photon count rates (x axis) as the pulse area varies within $0 < A \le \pi$

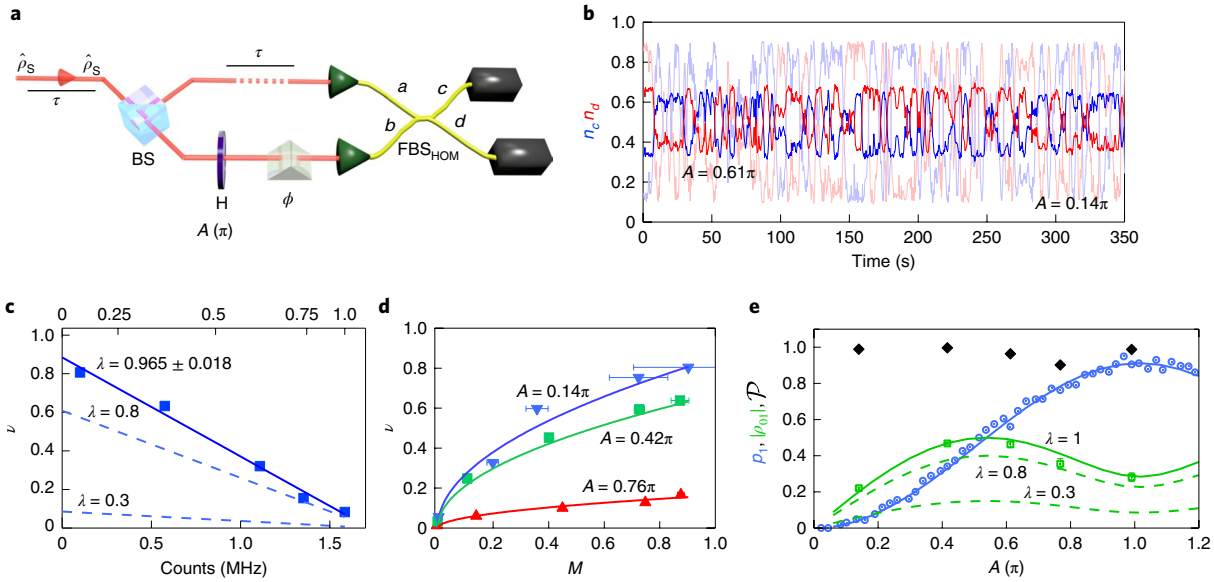

Fig. 2 | Quantum superposition of vacuum and one photon. a, Sketch of the MZI used to probe coherences in the photon number. The MZI delays one arm by $\tau = 12.34$ ns to allow interference of two consecutive wavepackets in the fibre beamsplitter FBS_{HOM}. The phase ϕ between the two arms of the MZI is not stabilized and thus it evolves freely in time. A half-wave plate H in one arm tunes the photon distinguishability via the polarization. **b**, Normalized single count rates n_c (blue) and n_d (red) for a pulse area $A = 0.61\pi$. Light blue (light red) traces display n_c (n_d) for $A = 0.14\pi$. Each data point here was accumulated for ~300 ms. **c**, Measured visibility v (blue squares) as a function of the count rates detected from our first collecting fibre. The blue solid line is a linear fit used to obtain the purity of the generated state and the dashed blue lines consider lower purity values. **d**, Visibility v in terms of the photon indistinguishability M (varied by polarization). Blue, green and red data points are taken for pulse areas A of 0.14π, 0.42π and 0.76π, respectively, and their corresponding curves follow the theoretical model $v = \lambda^2 p_0 \sqrt{M}$. **e**, Blue line, theoretical prediction for the probability p_1 of the QD to emit one photon. Blue data points, experimental one-photon population. Green solid line, theoretical prediction of the photon-number coherence amplitude ($|\rho_{01}| = \lambda\sqrt{p_0 p_1}$) assuming that the emitted state is pure ($\lambda = 1$). Dashed green lines, as for the solid line but for cases with less purity. Green data points, extracted values for $|\rho_{01}|$ deduced from the measured visibilities. Black data points, extracted values of purity $\mathcal{P}$. Error bars are obtained assuming Poissonian statistics in the detected events.

(top axis). We observe the expected increase in visibility when increasing the vacuum part. The visibility v also depends on the mean wavepacket overlap M, which is extracted from coincidence counts at the MZI output. We measured $M_\pi = 0.903 \pm 0.008$ with π-pulse excitation, a value limited both by residual pure dephasing[43] and a small residual phonon sideband[44], because no spectral filtering was used. In our model, we consider an effective dephasing term that accounts for both phenomena (see Supplementary Information).

We can then tune M via the relative photon polarization (Fig. 2d) and observe that the oscillation visibility vanishes for distinguishable photons, as expected. We observe that v is linear in the single-photon count rates (Fig. 2c), and accordingly proportional to vacuum, from which we deduce an average $\lambda = 0.965 \pm 0.018$ for all pulse areas up to π pulse. The state purity in the photon-number basis $\mathcal{P} = \mathrm{Tr}(\rho^2)$ is extracted knowing p_0, p_1 and λ. We obtain an average value of $\mathcal{P} = 0.968 \pm 0.008$ in the full $[0-\pi]$ pulse area range (Fig. 2e), evidencing the high degree of purity. These states are produced on demand: for each excitation pulse, the device emits a photon-number superposition, with $p_0 + p_1 = 1$.

To support the model described above, we consider the situation where a two-level system, with ground $|g\rangle$ and excited $|e\rangle$ states, is coupled to a single spatial mode of the optical field, that is, a one-dimensional (1D) atom[45], a model that has been shown to account well for the system under study[38]. Here, the cavity allows for the efficient collection of single photons, as well as accelerated spontaneous emission in the weak coupling regime that allows mitigation of the effect of pure dephasing and obtaining highly indistinguishable photonic states[20]. We calculate the light field generated by the QD by solving the Lindblad equation, which accounts for the evolution of a two-level system, treating the incoming laser field, the interaction unitary Hamiltonian, as well as the non-unitary dynamics of spontaneous emission and pure dephasing (see Supplementary Information). We obtain a system output state that can be written as the density matrix ρ_S. This matrix is time-integrated over the whole light pulse, an approach that is valid for excitation pulses well below the spontaneous emission time.

We theoretically obtain the population p_1 (respectively, p_0) and coherences $\lambda\sqrt{p_0 p_1}$ of ρ_S from parameters within the 1D atom model. Pure dephasing contributes to reducing the mean wavepacket overlap of the emitted photons, as well as the populations. The solid blue line in Fig. 2e shows the calculated populations p_1 and the solid green line the corresponding coherences for the case of maximally pure states ($\lambda = 1$).

Our observations report the on-demand direct generation of highly pure optical quantum states in the photon-number basis. Such photon-number quantum superpositions have been demonstrated for microwave photons, using quantum feedback with Rydberg atoms[46], or through synthesized methods using a superconducting phase qubit[47]. Here, the quantum superposition is directly obtained from the spontaneous emission of a quantum emitter. This is observed not only in the weak excitation regime[35]—that is, elastic scattering—where the atomic population nearly vanishes, but also up to population inversion. As a result, by adjusting the excitation pulse area, we can generate quantum superpositions of zero and one photon with controlled populations. We note that our measurements provide information about the purity of the quantum state at the output of the emitter. Imperfect photon extraction from the device or losses in the optical set-up have no impact on the presented interferometric measurements (see Supplementary

Information). In the next part, we study the case of even stronger driving, under a 2π-pulse area, and report on the generation of a quantum superposition of zero-, one- and two-photon Fock states.

Quantum superpositions up to two photons

Strong driving of the atom has been proposed as a means to generate photon bundles[48] and evidence for two-photon emission from an artificial atom has been reported recently by coherently driving a charged exciton at 2π pulse[41]. The excited-state population with a 2π-pulse drive is expected to be zero, unless some relaxation process takes place during the pulse. In particular, as long as the driving pulse duration is not infinitely short, the atom in its excited state shows a non-zero probability to undergo spontaneous emission during the pulse. In such a case, a first photon is spontaneously emitted, and the probability for a second excitation during the pulse is non-zero, leading to the emission of a second photon at the end of the excitation. See Supplementary Information for a description of the Rabi oscillations and the emission lifetime with a 2π-pulse drive.

The pronounced photon bunching observed at 2π-pulse excitation with our second device QD2 (Fig. 1d), quantified by $g^{(2)}_{2\pi}(0)=2.98\pm0.11$, shows that its emission at $A=2\pi$ contains non-zero two-photon terms. The generated light wavepacket is then composed of zero-, one- and two-photon Fock states. Indeed, it has been shown theoretically that higher-number terms should be negligible when the excitation pulse length is significantly shorter than the spontaneous emission time[41], a prediction that has been here confirmed with third-order correlation measurements (see Supplementary Information). We now argue that the generated state contains quantum coherences in the photon-number basis. Indeed, the experimental set-up depicted in Fig. 2a allows us to quantify the photon-number populations—including the two-photon component—and the degree of purity in this basis.

We learned from equation (1) that the counts of a single detector at the output of the path-unbalanced MZI interferometer carry information on the quantum coherence between the zero and one-photon Fock states. If we now consider the coincidence counts from the two output detectors as well, we show that we can obtain information on the purity in the number basis up to two photons. In general, we can extend the previous analysis and consider an input state ρ_S now containing terms up to the $|m\rangle$ Fock state. We consider a state with the same general form as before, that is, $\rho_S=\lambda\rho_{\text{pure}}+(1-\lambda)\rho_{\text{mixed}}$, in a simplified picture where the state impurity is described through a single parameter λ, reducing, here, all coherences in the same way. Within such a framework, it can be shown (see Supplementary Information) that the detected single-click count rates $\mathcal{N}_{c,d}$ at the interferometer outputs c and d (Fig. 2a) read

$$\mathcal{N}_{c,d}=\frac{1}{2}\left[\langle n\rangle\pm C_1\cos(\phi)\right] \tag{2}$$

where $\langle n\rangle=\sum_n^m np_n$ is the system mean photon number and $C_1=\lambda^2\left(\sum_n^m\sqrt{np_np_{n-1}}\right)^2$ is a first-order coherence term, with the summation indices hereafter from 0 to m, and λ accounts for the photon-number purity. The coincidence rate (at zero delay) follows

$$\mathcal{C}(0)=\frac{1}{8}\left[\langle n(n-1)\rangle-C_2\cos(2\phi)\right] \tag{3}$$

where $\langle n(n-1)\rangle=\sum_n^m n(n-1)p_n$ is the non-normalized second-order correlation function and $C_2=\lambda^2\left(\sum_n^m\sqrt{n(n-1)p_np_{n-2}}\right)^2$ is a coherence term of second order. Through equations (2) and (3), we obtain the normalized output coincidences at zero delay $\overline{\mathcal{C}}(0)=\mathcal{C}(0)/(\mathcal{N}_c\mathcal{N}_d)=\frac{1}{2}g^{(2)}(0)(1-v_2\cos2\phi)/(1-v_1^2\cos^2\phi)$, where $g^{(2)}(0)=\langle n(n-1)\rangle/\langle n\rangle^2$ is the normalized second-order correlation function of the input state, $v_1=C_1/\langle n\rangle$ is the single detector counts visibility and $v_2=C_2/\langle n(n-1)\rangle$ is the coincidences visibility. Equation (3) shows oscillations modulated at twice the phase dependence of equation (2): coherences in the photon number allow phase super-resolving interferometry.

The state generated at 2π-pulse driving contains up to two-photon terms, in which case we obtain $v_1=\lambda^2p_1(p_0+2\sqrt{2p_0p_2}+2p_2)/(p_1+2p_2)$, $v_2=\lambda^2p_0$ and $g^{(2)}(0)=2p_2/(p_1+2p_2)^2$. Thus, by measuring v_1, v_2, $g^{(2)}(0)$ and taking into account normalization $p_0+p_1+p_2=1$, we univocally determine p_0, p_1, p_2 and λ. Figure 3a,b shows our measurements for $n_c=\mathcal{N}_c/\langle n\rangle=(1+v_1\cos\phi)/2$ and coincidences proportional to $\mathcal{C}(0)\propto(1-v_2\cos(2\phi))$ with a rate specific to the losses of our set-up. Figure 3c shows our time-correlated coincidence measurements $\overline{\mathcal{C}}(\Delta t)$. As predicted, the coincidences at zero delay $\overline{\mathcal{C}}(0)$ oscillate with 2ϕ, with minima (maxima) of coincidences occurring for $\phi=0$ ($\phi=\pi/2$). The full phase span for $\overline{\mathcal{C}}(0)$ (modulo π) is shown in Fig. 3d. In the case of fully mixed (pure) states in the photon-number basis, that is, $\lambda=0$ ($\lambda=1$), oscillation visibilities in the coincidence counts fully vanish (maximally oscillate); see dashed grey (dot-dashed blue) curve in Fig. 3d.

We extract $v_1=0.192\pm0.008$, $v_2=0.452\pm0.038$, which together with the measured value of $g^{(2)}_{2\pi}(0)=2.98\pm0.11$ (Fig. 1d) and the normalization of probabilities, results in the distribution $\{p_n,\lambda\}$, with $p_0=0.838\pm0.012$, $p_1=0.051\pm0.002$, $p_2=0.111\pm0.010$ and $\lambda=0.734\pm0.025$. The generation of light states with $p_2>p_1$ is observed with charged excitons under a strong 2π-pulse drive of the QD (see Methods). The state $\rho_S^{2\pi}$ contains zero, one and two photons, with a quantum state purity of $\mathcal{P}=0.870\pm0.024$ (Fig. 3e). Interestingly, the temporal profile of this photonic state differs from standard mono-exponential decays obtained below π-pulse excitation, and instead displays a richer structure akin to previous theoretical predictions[41] (see Supplementary Information). Moreover, this profile also includes other interesting features, such as a delayed revival, most probably related to a richer dynamics within the four-level structure of the charged exciton, and its complete understanding therefore requires further theoretical and experimental investigation. Note that the theoretical analysis for the 2π-pulse drive considers the single-photon and two-photon components within the same mode in all degrees of freedom, including the temporal profile. Accordingly, it does not account for the effect of limited photon indistinguishability ($M<1$) or the presence of residual laser, as observed in the measured lifetime shown in the Supplementary Information. This reported purity for the 2π-pulse drive thus represents a lower bound for the photon-number purity alone.

This state, with $p_2>p_1$, incidentally resembles other quantum states of interest. The obtained photon distribution $\{p_n^{2\pi}\}$ presents a statistical fidelity $\mathcal{F}^{\text{cat}}=\sum_n\sqrt{p_n^{2\pi}p_n^{\text{cat}}}$ to $\{p_n^{\text{cat}}\}$, the probability distribution of an even 'Schrödinger-cat' state $|\text{cat}\rangle\propto|\alpha\rangle+|-\alpha\rangle$, where $|\alpha\rangle$ is a coherent state, of $\mathcal{F}^{\text{cat}}=0.974\pm0.016$ for a small cat state with $|\alpha|^2=0.5$. Thus, by simply driving a charged quantum dot with 2π pulses, we are able to generate other photonic states that may find applications in coherent-state driven quantum computation[49,50] and quantum metrology[51].

Conclusions

Quantum states with a high degree of purity are essential in all quantum-enhanced technologies. Optical quantum technologies have so far exploited various degrees of freedom, such as time frequency, angular momentum or polarization[1,2], but not the photon number due to the absence of suitable sources. Our work demonstrates that state-of-the-art semiconductor QD emitters not only provide high

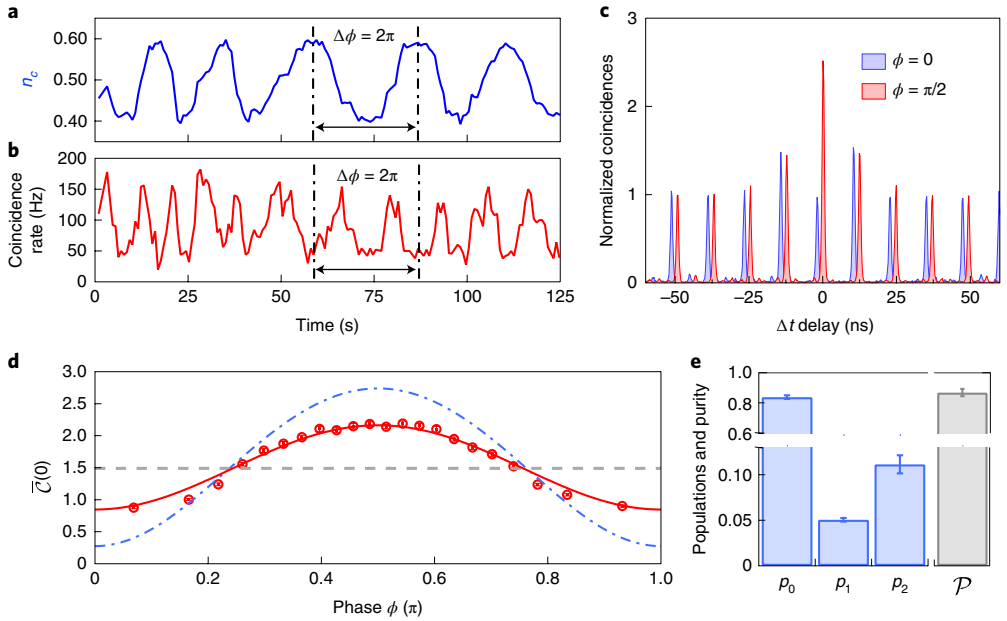

Fig. 3 | Quantum superposition of vacuum, one and two photons. a, Normalized single counts n_c as the phase ϕ freely evolves in time. **b**, Coincidence rate at zero delay evolving in time (full data were taken during 1,500 s), cycling twice per unit of interferometric phase cycle $\Delta\phi = 2\pi$—that is, showing phase super-resolution. **c**, Normalized time-correlated coincidences for a phase $\phi = 0$ (blue) and $\phi = \pi/2$ (red). **d**, Normalized coincidences at zero delay $\overline{\mathcal{C}}(0)$ (red circles) as a function of ϕ, with the theoretical prediction (red line) considering the extracted values of $\{p_n, \lambda\}$ described in **e**, and the expected predictions for the same Fock-state populations $\{p_n\}$ in the cases of maximally pure, that is, $\lambda = 1$ (blue dashed line), and classical statistical mixtures, that is, $\lambda = 0$ (grey dashed line). **e**, Populations $\{p_n\}$ and purity $\mathcal{P}$ of the emitted state at $A = 2\pi$. Error bars result from propagated Poissonian statistics.

purity in the frequency basis but also non-classical photon-number superpositions on demand. The generation of coherent superpositions of zero and one photon has been reproducibly observed for half a dozen devices, based either on neutral or charged exciton transitions, when exciting below the π pulse, and with high purity in the photon-number basis observed for both types of transition. Other non-classical states can also be generated by adjusting the excitation pulse duration and intensity. However, the generation of light with $p_2 > p_1$ is only observed when driving charged excitons with 2π pulses, and it is not observed with neutral excitons. Indeed, in a crossed-polarization collection scheme, the observed neutral exciton signal is time-delayed by the fine-structure splitting[38], bypassing re-excitations during the same pulse.

We believe that the generation of quantum superpositions of photon numbers opens new exciting routes for optical quantum technologies. For example, we can now exploit the interference of these novel photonic states, potentially impacting the complexity of existing quantum-enhanced protocols, such as in quantum computing or quantum walks.

Online content

Any methods, additional references, Nature Research reporting summaries, source data, statements of code and data availability and associated accession codes are available at https://doi.org/10.1038/s41566-019-0506-3.

Received: 3 December 2018; Accepted: 7 July 2019;
Published online: 19 August 2019

References

1. O'Brien, J. L., Furusawa, A. & Vučković, J. Photonic quantum technologies. *Nat. Photon.* **3**, 687–695 (2009).
2. Erhard, M., Fickler, R., Krenn, M. & Zeilinger, A. Twisted photons: new quantum perspectives in high dimensions. *Light Sci. Appl.* **7**, 17146 (2018).
3. Waks, E., Diamanti, E. & Yamamoto, Y. Generation of photon number states. *New J. Phys.* **8**, 4 (2006).
4. Pan, J.-W. et al. Multiphoton entanglement and interferometry. *Rev. Mod. Phys.* **84**, 777–838 (2012).
5. Wang, X.-L. et al. Experimental ten-photon entanglement. *Phys. Rev. Lett.* **117**, 210502 (2016).
6. Scarani, V. et al. The security of practical quantum key distribution. *Rev. Mod. Phys.* **81**, 1301–1350 (2009).
7. Bunandar, D. et al. Metropolitan quantum key distribution with silicon photonics. *Phys. Rev. X* **8**, 021009 (2018).
8. Brida, G., Genovese, M. & Ruo Berchera, I. Experimental realization of sub-shot-noise quantum imaging. *Nat. Photon.* **4**, 227–230 (2010).
9. Schwartz, O. et al. Superresolution microscopy with quantum emitters. *Nano Lett.* **13**, 5832–5836 (2013).
10. Knill, E., Laamme, R. & Milburn, G. J. A scheme for efficient quantum computation with linear optics. *Nature* **409**, 46–52 (2001).
11. O'Brien, J. L. Optical quantum computing. *Science* **318**, 1567–1570 (2007).
12. Lanyon, B. P. et al. Towards quantum chemistry on a quantum computer. *Nat. Chem.* **2**, 106–111 (2010).
13. Loredo, J. C. et al. Measuring entanglement in a photonic embedding quantum simulator. *Phys. Rev. Lett.* **116**, 070503 (2016).
14. Chen, M.-C. et al. Efficient measurement of multiparticle entanglement with embedding quantum simulator. *Phys. Rev. Lett.* **116**, 070502 (2016).
15. Santagati, R. et al. Witnessing eigenstates for quantum simulation of Hamiltonian spectra. *Sci. Adv.* **4**, eaap9646 (2018).
16. O'Brien, J. L., Pryde, G. J., White, A. G., Ralph, T. C. & Branning, D. Demonstration of an all-optical quantum controlled-NOT gate. *Nature* **426**, 264–267 (2003).
17. Patel, R. B., Ho, J., Ferreyrol, F., Ralph, T. C. & Pryde, G. J. A quantum Fredkin gate. *Sci. Adv.* **2**, e1501531 (2016).
18. Wang, X.-L. et al. Quantum teleportation of multiple degrees of freedom of a single photon. *Nature* **518**, 516–519 (2015).
19. Takeda, S., Fuwa, M., van Loock, P. & Furusawa, A. Entanglement swapping between discrete and continuous variables. *Phys. Rev. Lett.* **114**, 100501 (2015).
20. Somaschi, N. et al. Near-optimal single-photon sources in the solid state. *Nat. Photon.* **10**, 340–345 (2016).
21. Ding, X. et al. On-demand single photons with high extraction efficiency and near-unity indistinguishability from a resonantly driven quantum dot in a micropillar. *Phys. Rev. Lett.* **116**, 020401 (2016).
22. Senellart, P., Solomon, G. & White, A. High-performance semiconductor quantum-dot single-photon sources. *Nat. Nanotechnol.* **12**, 1026–1039 (2017).

23. Kirsanske, G. et al. Indistinguishable and efficient single photons from a quantum dot in a planar nanobeam waveguide. *Phys. Rev. B* **96**, 165306 (2017).
24. Lombardi, E., Sciarrino, F., Popescu, S. & De Martini, F. Teleportation of a vacuum-one-photon qubit. *Phys. Rev. Lett.* **88**, 070402 (2002).
25. Gabriel, C. et al. A generator for unique quantum random numbers based on vacuum states. *Nat. Photon.* **4**, 711–715 (2010).
26. Bimbard, E., Jain, N., MacRae, A. & Lvovsky, A. I. Quantum-optical state engineering up to the two-photon level. *Nat. Photon.* **4**, 243–247 EP (2010).
27. Fuwa, M., Takeda, S., Zwierz, M., Wiseman, H. M. & Furusawa, A. Experimental proof of nonlocal wavefunction collapse for a single particle using homodyne measurements. *Nat. Commun.* **6**, 6665 (2015).
28. Grangier, P., Roger, G. & Aspect, A. Experimental evidence for a photon anticorrelation effect on a beam splitter: a new light on single-photon interferences. *Europhys. Lett.* **1**, 173–179 (1986).
29. Lounis, B. & Moerner, W. E. Single photons on demand from a single molecule at room temperature. *Nature* **407**, 491–493 (2000).
30. Michler, P. et al. A quantum dot single-photon turnstile device. *Science* **290**, 2282–2285 (2000).
31. Michler, P. et al. Quantum correlation among photons from a single quantum dot at room temperature. *Nature* **406**, 968–970 (2000).
32. Jessen, P. S. et al. Observation of quantized motion of Rb atoms in an optical field. *Phys. Rev. Lett.* **69**, 49–52 (1992).
33. Nguyen, H. S. et al. Ultra-coherent single photon source. *Appl. Phys. Lett.* **99**, 261904 (2011).
34. Matthiesen, C., Vamivakas, A. N. & Atature, M. Subnatural linewidth single photons from a quantum dot. *Phys. Rev. Lett.* **108**, 093602 (2012).
35. Matthiesen, C. et al. Phase-locked indistinguishable photons with synthesized waveforms from a solid-state source. *Nat. Commun.* **4**, 1600 (2013).
36. Proux, R. et al. Measuring the photon coalescence time window in the continuous-wave regime for resonantly driven semiconductor quantum dots. *Phys. Rev. Lett.* **114**, 067401 (2015).
37. Schulte, C. H. H. et al. Quadrature squeezed photons from a two-level system. *Nature* **525**, 222–225 (2015).
38. Giesz, V. et al. Coherent manipulation of a solid-state artificial atom with few photons. *Nat. Commun.* **7**, 11986 (2016).
39. Dousse, A. et al. Controlled light–matter coupling for a single quantum dot embedded in a pillar microcavity using far-field optical lithography. *Phys. Rev. Lett.* **101**, 267404 (2008).
40. Nowak, A. K. et al. Deterministic and electrically tunable bright single-photon source. *Nat. Commun.* **5**, 3240 (2014).
41. Fischer, K. A. et al. Signatures of two-photon pulses from a quantum two-level system. *Nat. Phys.* **13**, 649–654 (2017).
42. Hong, C. K., Ou, Z. Y. & Mandel, L. Measurement of subpicosecond time intervals between two photons by interference. *Phys. Rev. Lett.* **59**, 2044–2046 (1987).
43. Fischer, K. A., Trivedi, R. & Lukin, D. Particle emission from open quantum systems. *Phys. Rev. A* **98**, 023853 (2018).
44. Grange, T. et al. Reducing phonon-induced decoherence in solid-state single-photon sources with cavity quantum electrodynamics. *Phys. Rev. Lett.* **118**, 253602 (2017).
45. Valente, D. et al. Monitoring stimulated emission at the single-photon level in one-dimensional atoms. *Phys. Rev. A* **85**, 023811 (2012).
46. Sayrin, C. et al. Real-time quantum feedback prepares and stabilizes photon number states. *Nature* **477**, 73–77 (2011).
47. Hofheinz, M. et al. Synthesizing arbitrary quantum states in a superconducting resonator. *Nature* **459**, 546–549 (2009).
48. Munoz, C. S. et al. Emitters of *n*-photon bundles. *Nat. Photon.* **8**, 550–555 (2014).
49. Ralph, T. C., Gilchrist, A., Milburn, G. J., Munro, W. J. & Glancy, S. Quantum computation with optical coherent states. *Phys. Rev. A* **68**, 042319 (2003).
50. Lund, A. P., Ralph, T. C. & Haselgrove, H. L. Fault-tolerant linear optical quantum computing with small-amplitude coherent states. *Phys. Rev. Lett.* **100**, 030503 (2008).
51. Gilchrist, A. et al. Schrödinger cats and their power for quantum information processing. *J. Opt. B* **6**, 5828–5833 (2004).

Acknowledgements

This work was partially supported by ERC Starting Grant no. 277885 QD-CQED, the French Agence Nationale pour la Recherche (grant ANR SPIQE and USSEPP), the French RENATECH network and a public grant overseen by the French National Research Agency (ANR) as part of the Investissements d'Avenir programme (Labex NanoSaclay, reference ANR-10-LABX-0035). J.C.L. and C.A. acknowledge support from Marie Skłodowska-Curie Individual Fellowships SMUPHOS and SQUAPH, respectively. We thank N. Carlon Zambon for providing technical assistance throughout the project.

Author contributions

The experiments were conducted by J.C.L. and C.A. with help from P.H., C.M., H.O. and L.D.S. Data analysis was carried out by C.A. and J.C.L. The theoretical modelling was done by A.A., B.R., O.K., C.A. and J.C.L. The cavity devices were fabricated by A.H. and N.S. from samples grown by A.L., and the etching was done by I.S. The manuscript was written by J.C.L., C.A. and P.S. with input from all authors. The project was supervised by L.L., A.A., O.K. and P.S.

Competing interests

N.S. is co-founder, and P.S. is scientific advisor and co-founder, of the single-photon-source company Quandela.

Additional information

Supplementary information is available for this paper at https://doi.org/10.1038/s41566-019-0506-3.

Reprints and permissions information is available at www.nature.com/reprints.

Correspondence and requests for materials should be addressed to J.C.L., C.A. or P.S.

Publisher's note: Springer Nature remains neutral with regard to jurisdictional claims in published maps and institutional affiliations.

Methods

Sample. The microcavity samples were grown by molecular beam epitaxy. A λ-GaAs cavity was surrounded by bottom and top mirrors composed of 30 and 20 pairs of GaAs/$Al_{0.9}Ga_{0.1}As$, respectively. The mirrors were gradually n- and p-doped to tune the QD transition through the confined Stark effect. The cavities were centred on the QDs using an in situ optical lithography technique[39]. The sample was then etched and standard p-contacts were defined on a large frame ($300\times300\,\mu m^2$) connected to the circular frame around the micropillar. A standard n-contact was defined on the sample back surface. A neutral exciton was coupled to the cavity mode for QD1. For optical measurements, the polarization of the laser was set so that the fine-structure splitting resulted in emission in crossed polarization[38]. A positively charged exciton was coupled to the cavity mode for QD2, and in this case the circular polarization and optical transition rules naturally allowed us to obtain a signal in the crossed-polarization configuration. QD1 (QD2) was excited resonantly with linearly polarized 40 ps (15 ps) laser pulses at 925 nm. The pulse lengths were chosen to minimize the $g^{(2)}(0)$ values up to the π pulse. A longer pulse was used for QD1 because the collection in crossed polarization was time-delayed by the slow polarization rotation induced by the exciton fine-structure splitting[38]. Such a temporally long, and therefore spectrally narrow, pulse is easier to suppress in a crossed-polarization scheme. For the charged exciton, conversely, the spontaneous emission in crossed polarization was collected immediately upon excitation, so a shorter pulse length was required to obtain low $g^{(2)}(0)$ values.

Time-tagged correlation measurements. Simultaneous acquisition of single counts and double coincidences were recorded by measuring the photon count rate and photon event time tags in the output detectors (Si avalanche photodiodes) of the MZI, which were connected to a computer-controlled HydraHarp 400 autocorrelator.

Under free evolution of the phase ϕ between the two arms of the MZI, the total acquisition time per point was set to $T_{acq}=310$ ms (810 ms) for the results described in Fig. 2 (Fig. 3), with an integration time for the photon time tags of $T_{TT}=200$ ms (500 ms). Given the relatively fast acquisition of experimental points, the phase ϕ remained approximately unchanged during each acquisition run. The measurement protocol for each data point was as follows: the Hydraharp autocorrelator read the laser clock signal (24.6700 ± 0.0026 ns), a period of time that served as a reference to determine the photon time tags of the detected events (accumulated during T_{TT}); consecutively, during the interval $T_{acq}-T_{TT}$, the count rates in the APDs were averaged and the phase ϕ eventually obtained (see Supplementary Information).

Data analysis. The outcome of the time-tagged measurements rendered the count rates and two-photon coincidences as a function of time (the total integration time was on the order of 10–15 min for a given pulse area and relative photon polarization in the MZI). From the oscillation of the single counts, an intensity-to-phase mapping was used to organize the phase-dependent two-photon coincidences as function of the relative phase ϕ. We used the normalized intensity counts, for example n_c, to assign a corresponding ϕ value for each given acquisition time bin. For example, at a given time bin, the n_c values that were the maximum, minimum or equal to n_d were mapped to phases ϕ equal to 0, π or $\pi/2$, respectively. See Supplementary Information for further explanations.

Data availability

The data that support the plots within this paper and other findings of this study are available from the corresponding author upon reasonable request.

Terms and Conditions

Springer Nature journal content, brought to you courtesy of Springer Nature Customer Service Center GmbH (“Springer Nature”).
Springer Nature supports a reasonable amount of sharing of research papers by authors, subscribers and authorised users (“Users”), for small-scale personal, non-commercial use provided that all copyright, trade and service marks and other proprietary notices are maintained. By accessing, sharing, receiving or otherwise using the Springer Nature journal content you agree to these terms of use (“Terms”). For these purposes, Springer Nature considers academic use (by researchers and students) to be non-commercial.
These Terms are supplementary and will apply in addition to any applicable website terms and conditions, a relevant site licence or a personal subscription. These Terms will prevail over any conflict or ambiguity with regards to the relevant terms, a site licence or a personal subscription (to the extent of the conflict or ambiguity only). For Creative Commons-licensed articles, the terms of the Creative Commons license used will apply.
We collect and use personal data to provide access to the Springer Nature journal content. We may also use these personal data internally within ResearchGate and Springer Nature and as agreed share it, in an anonymised way, for purposes of tracking, analysis and reporting. We will not otherwise disclose your personal data outside the ResearchGate or the Springer Nature group of companies unless we have your permission as detailed in the Privacy Policy.
While Users may use the Springer Nature journal content for small scale, personal non-commercial use, it is important to note that Users may not:

1. use such content for the purpose of providing other users with access on a regular or large scale basis or as a means to circumvent access control;
2. use such content where to do so would be considered a criminal or statutory offence in any jurisdiction, or gives rise to civil liability, or is otherwise unlawful;
3. falsely or misleadingly imply or suggest endorsement, approval , sponsorship, or association unless explicitly agreed to by Springer Nature in writing;
4. use bots or other automated methods to access the content or redirect messages
5. override any security feature or exclusionary protocol; or
6. share the content in order to create substitute for Springer Nature products or services or a systematic database of Springer Nature journal content.

In line with the restriction against commercial use, Springer Nature does not permit the creation of a product or service that creates revenue, royalties, rent or income from our content or its inclusion as part of a paid for service or for other commercial gain. Springer Nature journal content cannot be used for inter-library loans and librarians may not upload Springer Nature journal content on a large scale into their, or any other, institutional repository.
These terms of use are reviewed regularly and may be amended at any time. Springer Nature is not obligated to publish any information or content on this website and may remove it or features or functionality at our sole discretion, at any time with or without notice. Springer Nature may revoke this licence to you at any time and remove access to any copies of the Springer Nature journal content which have been saved.
To the fullest extent permitted by law, Springer Nature makes no warranties, representations or guarantees to Users, either express or implied with respect to the Springer nature journal content and all parties disclaim and waive any implied warranties or warranties imposed by law, including merchantability or fitness for any particular purpose.
Please note that these rights do not automatically extend to content, data or other material published by Springer Nature that may be licensed from third parties.
If you would like to use or distribute our Springer Nature journal content to a wider audience or on a regular basis or in any other manner not expressly permitted by these Terms, please contact Springer Nature at

onlineservice@springernature.com